ARTICLE IN PRESS – J. Appl. Cryst.

ISSN 1600-5767

Neutron diffraction study of $(K_xNa_{1-x})NbO_3$-based ceramics from low to high temperatures

Proof instructions

Proof corrections should be returned by **28 April 2016**. After this period, the Editors reserve the right to publish your article with only the Managing Editor's corrections.

Please
(1) Read these proofs and assess whether any corrections are necessary.
(2) Check that any technical editing queries highlighted in **bold underlined** text have been answered.
(3) Send corrections by e-mail to **ls@iucr.org**. Please describe corrections using plain text, where possible, giving the line numbers indicated in the proof. Please do not make corrections to the pdf file electronically and please do not return the pdf file. If no corrections are required please let us know.

If you wish to make your article **open access** or purchase printed offprints, please complete the attached order form and return it by e-mail as soon as possible.

Please check the following details for your article

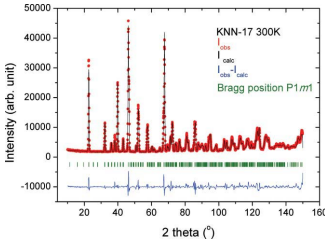

Thumbnail image for contents page

Synopsis: A low- to high-temperature neutron diffraction study of some $(K_xNa_{1-x})NbO_3$-based ceramics has been carried out. The structure of these ceramic compositions has been determined using Rietveld refinement.

Abbreviated author list: Mgbemere, H.; Schneider, G.; Hoelzel, M.; Hinterstein, M.

Keywords: neutron diffraction; $(K_xNa_{1-x})NbO_3$ ceramics; Rietveld refinement; temperature

How to cite your article in press

Your article has not yet been assigned page numbers, but may be cited using the doi:

Mgbemere, H., Schneider, G., Hoelzel, M. & Hinterstein, M. (2016). *J. Appl. Cryst.* **49**, doi:10.1107/S1600576716005197.

You will be sent the full citation when your article is published and also given instructions on how to download an electronic reprint of your article.

JOURNAL OF APPLIED CRYSTALLOGRAPHY

ISSN 1600-5767

Received 2 October 2015
Accepted 27 March 2016

Edited by G. Kostorz, ETH Zurich, Switzerland

Keywords: neutron diffraction; $(K_xNa_{1-x})NbO_3$ ceramics; Rietveld refinement; temperature.

Supporting information: this article has supporting information at journals.iucr.org/j

Neutron diffraction study of $(K_xNa_{1-x})NbO_3$-based ceramics from low to high temperatures

Henry Mgbemere,[a,b]* Gerold Schneider,[b] Markus Hoelzel[c] and Manuel Hinterstein[d,e]

[a]Department of Metallurgical and Materials Engineering, University of Lagos, Akoka, Lagos, Nigeria, [b]Institute of Advanced Ceramics, Hamburg University of Technology, Denickestrasse 15, Hamburg 21073, Germany, [c]Heinz Maier Leibnitz Zentrum (MLZ), Technische Universität München, Garching 85748, Germany, [d]School of Materials Science and Engineering, UNSW Australia, 2052 Sydney, Australia, and [e]Institute for Applied Materials, Karlsruhe Institute for Technology, PO Box 3640, Karlsruhe, 76021, Germany. *Correspondence e-mail: hmgbemere@unilag.edu.ng

A neutron diffraction study of $(K_xNa_{1-x})NbO_3$-based ceramics has been carried out from 5 K to high temperatures well above the Curie temperature. The diffraction data were analysed using Rietveld refinement. For pure KNN samples, especially at the Na-rich side of the phase diagram, the low-temperature structure of simple rhombohedral symmetry changes to a highly complex monoclinic structure at a higher temperature. Chemical analysis on the samples showed good agreement of the expected and actual compositions. Trigonal, monoclinic, orthorhombic, tetragonal and cubic phase models as well as two-phase mixtures are observed depending on the temperature of measurement. Space groups *R*3*c*, *P*1*m*1, *P*11*m*, *Amm*2, *P*4*mm*, $Pm\bar{3}m$ and their combinations are used to refine the trigonal, monoclinic, orthorhombic, tetragonal, cubic and mixed phases, respectively. For the $(K_{0.48}Na_{0.48}Li_{0.04})$-$(Nb_{0.86}Ta_{0.1}Sb_{0.04})O_3$ sample at temperatures between 5 and 300 K, the monoclinic *P*11*m* space group gives the best refinement fit. For the $(K_{0.17}Na_{0.83})NbO_3$ sample, a two-phase refinement using the trigonal *R*3*c* and monoclinic *Pm* space groups gave the best fit **at 300 K, while at 5–150 K** the trigonal *R*3*c* space group gives the best fit. The understanding of the structure of these lead-free ceramics will help in the optimization of their piezoelectric properties.

1. Introduction

$(K_xNa_{1-x})NbO_3$ (KNN) is a solid solution of $NaNbO_3$ and $KNbO_3$ and is of interest to researchers because of its potential to replace the currently used lead-based piezoelectric ceramics. The earliest phase diagram and crystal structures were obtained from temperature-dependent dielectric measurements and X-ray diffraction studies (Shirane *et al.*, 1954). Since then the piezoelectric, dielectric and electromechanical properties of KNN ceramics have been widely investigated (Egerton & Dillon, 1959; Jaeger & Egerton, 1962; Haertling, 1967). The presence and position of different phase boundaries were first reported by Tennery (1968) using calorimetric studies of enthalpy and entropy changes. Using X-ray diffraction, the lattice parameters, the tilting of the oxygen octahedra and the sequence of phase transitions have also been reported (Ahtee & Glazer, 1976). The tilting of the oxygen octahedra in perovskite materials is normally represented using the notation proposed by Glazer (1972). Ahtee & Hewat (1975) using neutron diffraction have studied the structure of KNN ceramics containing different potassium amounts (x = 0.02 and 0.1). The structural phase

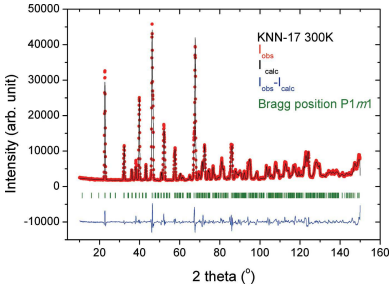

transitions were reported both at room temperature and at higher temperatures (Ahtee & Hewat, 1978).

Other characterization techniques have been used in recent times to investigate the structure of KNN ceramics. With Raman spectroscopy, it has been shown that the particle size of KNN ceramics influences the type of phase present (Shiratori *et al.*, 2005). When the particle size is <200 nm, a triclinic phase is observed, while when it is >200 nm, a monoclinic phase is observed. The symmetry of KNN ceramics with different sintering temperatures and holding times investigated with transmission electron microscopy (TEM) revealed that the crystal planes of the grains around the intragranular pores are of the {100} family, which are assumed to have the lowest surface energy (Jenko *et al.*, 2005). On the basis of TEM analysis, KNN single crystals were reported to have monoclinic symmetry at room temperature (Lallart, 2011).

The local atomic structure of KNN ceramics up to the third shell around the Nb atoms (x = 0–0.65) has been studied from low to high temperatures using Nb K edge extended X-ray absorption fine structure analysis (EXAFS), and the result shows that the distribution of Nb atoms on the surface changes during phase transitions (Lemeshko *et al.*, 2007). The geometry of the NbO_6 octahedra depends not on the **value of K [the value of x? the fraction of K?]** at each temperature but on the rotation of the octahedral Nb—O—Nb angle. In another EXAFS study, over a range of phase transitions, the Nb atoms were found to be displaced from the centre of the octahedra of their immediate oxygen neighbours through splitting of the Nb—O distances, with high displacements in the [111] crystallographic directions (Kodre *et al.*, 2009). Investigations of both KNN single crystals and ceramics by Baker *et al.* (2009*b*) have led to a modification of the phase diagram. On the basis of the tilt system and cation displacements as a function of temperature, the most significant structural change in KNN occurs when x = 0.2. Low-temperature structural investigations of KNN using neutron diffraction (x = 0.05 and 0.3) showed that rhombohedral $R3c$ structure and tilt system $a^-a^-a^-$ are present at room temperature. When x = 0.05, a two-phase coexistence between a monoclinic and a rhombohedral phase was observed (Zhang *et al.*, 2009).

The report by Saito *et al.* (2004) about KNN ceramics modified with Li, Ta and Sb showing much improved piezoelectric properties renewed a lot of interest in the topic. Several research results on these KNN-based ceramics have been reported. The increase in piezoelectric properties was attributed in part to the coexistence of the orthorhombic and tetragonal phases and has also been investigated with synchrotron X-ray diffraction (Mgbemere, Fernandes *et al.*, 2011; Mgbemere, Hinterstein & Schneider, 2011, 2012, 2013). According to Akdoğan *et al.* (2008) this phase coexistence is expected on the basis of Gibb's phase rule under isothermal and isobaric conditions. Rubio-Marcos *et al.* (2011) attributed it to the diffusion of the tetragonal phase and inhomogeneity in the composition. In the Raman stretching modes, the relation between structure, properties and the effective ionic displacement which leads to polarization were established (Rubio-Marcos *et al.* (2011).

Neutron diffraction is a valuable tool in the study of the structure of KNN ceramics because it gives a lot of information on the oxygen matrix owing to the high scattering cross section of oxygen compared to the X-ray atomic form factor. Therefore, precise determination of oxygen octahedral tilting is possible. There are only a few reports on the study of the structure of KNN ceramics from low temperatures to high temperatures using diffraction. Because of their minimal piezoelectric properties, the phase boundaries in KNN where x = 0.17 and 0.35, respectively, have not been investigated as they should be. There has also been little or no investigation of KNN ceramics containing Li, Ta and Sb using neutron diffraction. The objective of this paper is to study the structure of KNN ceramics at these phase boundaries (x = 0.17 and 0.35) as well as KNN ceramics modified with Li, Ta and Sb, using neutron diffraction in order to understand how the changes in composition and temperature affect the structure. The results will be significant for the development and optimization of KNN and other new lead-free piezoceramics, as a detailed knowledge of the crystal structure allows for tailoring of the electromechanical properties.

2. Experimental procedure

The samples were produced using the conventional mixed-oxide synthesis approach. The synthesis details for the KNN sample modified with Li, Ta and Sb, $(K_{0.48}Na_{0.48}Li_{0.04})(Nb_{0.86}Ta_{0.1}Sb_{0.04})O_3$, here abbreviated as KNNLST, have been reported in the literature (Mgbemere *et al.*, 2009*a*), while for $(K_{0.17}Na_{0.83})NbO_3$ and $(K_{0.35}Na_{0.65})NbO_3$ compositions, K_2CO_3, Na_2CO_3 and Nb_2O_5 were used as the starting powders. The powders were mixed and attrition milled for 2 h at 500 r mine^{-1} using zirconia balls as grinding media and ethanol as solvent. The powders were then calcined at 1123 K for 4 h, and after the calcination, the milling process was repeated using the same process parameters. The powders were pressed into tablets of approximately 13 mm diameter by 12 mm thickness with a uniaxial press at 75 MPa for 30 s and with a cold isostatic press at 300 MPa for 2 min. The samples were sintered in air atmosphere at temperatures between 1373 and 1453 K for 1 h. The density was measured using the Archimedes method, and grinding and polishing of the sample were done in preparation for the measurements. The chemical analysis of the sample after sintering was carried out using an optical emission spectroscopy/inductive coupled plasma (OES/ICP) device (PE-Optima 7000 DV).

2.1. Neutron diffraction data collection and refinement

The neutron powder diffraction measurements were carried out with the powder diffractometer SPODI at the research reactor FRM II of the Heinz Maier-Leibnitz Zentrum (Garching near Munich, Germany) (Hoelzel *et al.*, 2012) with an incident wavelength of 1.548 Å. Low-temperature measurements were performed using a closed cycle cryostat

from 5 to 300 K. Temperature intervals of approximately 150 K were chosen for the measurements to correspond to the occurrence of different phases in the samples. The high-temperature measurements were made *in situ* in a high-temperature vacuum furnace from 300 K up to 976 K. The patterns were collected using a bank of 80 position-sensitive ^{3}He detectors which covers a 160° scattering range. The wavelength and instrumental profile were determined using a corundum standard. The samples have a cylindrical form with a height of ∼10 mm and a diameter of ∼10 mm.

The Rietveld method as implemented in the *Fullprof* suite (Rodríguez-Carvajal, 2001) was used to refine all the collected data. The following phases were used for the refinement: rhombohedral (*R*3*c*), monoclinic (*P*1*m*1), monoclinic (*P*11*m*), orthorhombic (*Amm*2), tetragonal (*P*4*mm*) and cubic ($Pm\bar{3}m$). The criteria for choosing the various models used in the refinement, whether a single-phase model or a two-phase model is used, are based on the obtained agreement factors of the fit. This decision is also guided by prior knowledge of the $KNbO_3$ – $NaNbO_3$ system and low *R* values. A two-phase model is used where a combination of the phases results in lower *R* values and better goodness of fit. The background was refined using a linear interpolation between points from the regions where no reflections contributed to the intensities. A Thompson–Cox–Hastings pseudo-Voigt profile function, which is convoluted with asymmetry owing to axial divergence as formulated by Laar & Yelon (1984) and using the method of Finger (Finger *et al.*, 1994; Finger, 1998), is used for the model. The atomic positions were refined for the oxygen atoms and *B*-site cations, while the isotropic atomic displacement parameters B_{iso} were refined for all the elements.

3. Results and discussion

The result of the chemical analysis on the samples is shown in Table 1. The actual amount represents the mean value from four separate measurements, while the expected amounts are based on calculations from the stoichiometric composition. The actual and expected amounts of the sample with composition $(K_{0.17}Na_{0.83})NbO_3$ are similar with only very small differences. The actual amount of oxygen is lower than expected, and this could be because of the atmosphere used during sintering, where there was insufficient oxygen for the process. The alkali elements Na and K are known to volatilize during sintering, and to compensate for their volatility, 3% excess was added to the starting powder. For the sample with composition $(K_{0.35}Na_{0.65})NbO_3$, the actual and expected amounts of K are very similar but the amount of Na was higher than expected. This can be explained by the fact that less Na than anticipated was lost during sintering. For the KNNLST sample, the difference between the actual and expected element amounts is minimal, thereby confirming that the composition of the sample produced matches what is expected. The trace Zr in the analysis is from the ZrO_2 balls used during milling, and this is as a result of friction between the grinding balls and the powder.

Table 1
Actual and expected amounts of the elements in the samples analysed using the OES/ICP technique.

Element	Li	Na	K	Nb	Ta	Sb	O	Zr
$K_{0.17}Na_{0.83}NbO_3$								
Expected amount (mol)		0.83	0.17	1			3	
Actual amount (mol)		0.818	0.173	1.091			2.918	
$K_{0.35}Na_{0.65}NbO_3$								
Expected amount (mol)		0.65	0.35	1			3	
Actual amount (mol)		0.734	0.34	0.968			2.957	0.0008
$(K_{0.48}Na_{0.48}Li_{0.04})(Nb_{0.86}Ta_{0.1}Sb_{0.04})O_3$								
Expected amount (mol)	0.04	0.48	0.48	0.86	0.1	0.04	3	
Actual amount (mol)	0.034	0.508	0.476	0.85	0.099	0.038	2.994	0.0008

3.1. $(K_{0.17}Na_{0.83})NbO_3$ ceramics from 5 to 976 K

The lead-free composition $(K_{0.17}Na_{0.83})NbO_3$ is situated at one of the phase boundary lines in the $KNbO_3$–$NaNbO_3$ system. Because of the difficulty associated with sample preparation and sintering, there is little or no information in the literature about its properties. The measurement of the ferroelectric properties can be challenging owing to the high conductivity under an applied electric field. The Curie temperature of the sample is approximately 691 K, while its dielectric constant value at 1 kHz is approximately 350 with a dielectric loss value as high as 0.5.

The neutron powder diffraction patterns for $(K_{0.17}Na_{0.83})NbO_3$ ceramics from 5 to 776 K are shown in Fig. 1. The diffraction pattern at 976 K is very similar to that at 776 K and so is not presented here. The right-hand panel is an enlargement of the pattern from 37 to 41° to highlight the presence of superlattice reflections in the sample originating from in-phase or anti-phase tilting of the oxygen octahedra. As the temperature of data acquisition increases, the patterns gradually change, reflecting structural transitions from the rhombohedral phase at 5 K through the monoclinic phase

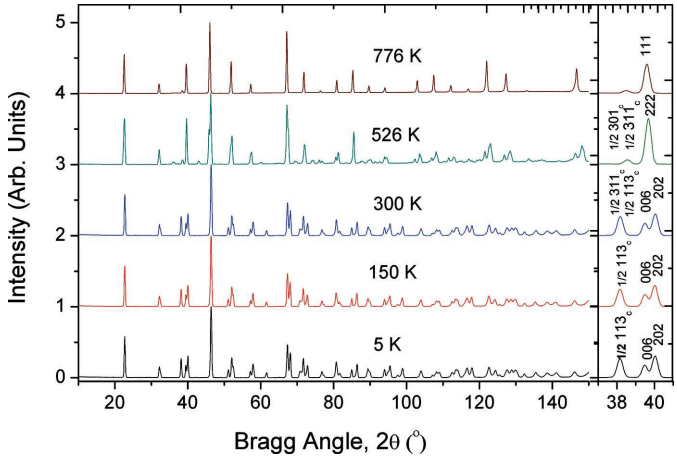

Figure 1
Neutron powder diffraction (λ = 1.5484 Å) patterns of $(K_{0.17}Na_{0.83})NbO_3$ at 5, 150, 300, 526 and 776 K. The right-hand panel shows some of the tilt peaks in the patterns between 37 and 41°, from 5 K to temperatures up to 526 K. The subscript 'c' refers to the pseudocubic indexing of the unit cell.

Table 2
Table showing the refinement details for all the possible models investigated for $(K_{0.17}Na_{0.83})NbO_3$ ceramics from 5 to 976 K.

The models that were actually selected are shown in bold.

Temperature (K)	Space group	R_p	R_{wp}	χ^2	R_{Bragg}
5	***R3c***	**7.88**	**8.96**	**12.2**	**3.07**
150	***R3c***	**8.18**	**9.22**	**12.2**	**3.34**
300	*P*1*m*1	14.3	15.9	28.8	6.49
300	***P1m1***	**9.39**	**10.3**	**11.9**	**5.45**
	R3c				**5.96**
300	*R3c*	32.4	33.2	114	9.54
526	*P*1*m*1	11.7	13.3	22	6.88
526	***P1m1***	**10.7**	**12.4**	**19.6**	**5.94**
	R3c				**14.6**
776	***Pm3m***	**15.3**	**17.4**	**44.9**	**6.93**
976	***Pm3m***	**15.3**	**17.1**	**40.1**	**7.74**

around room temperature and finally to the cubic phase at 776 K.

The measured and calculated diffraction profiles together with their difference plots for two structure models for $(K_{0.17}Na_{0.83})NbO_3$ ceramics at 300 K are shown in Fig. 2.

A two-phase monoclinic–rhombohedral (*P*1*m*1 + *R*3*c*) model was used to describe the measured diffraction data (Fig. 2*a*). Attempts to use only either *P*1*m*1 or *R*3*c* single-phase models resulted in higher *R* values and a poorer fit. As a comparison, the fit with a single-phase monoclinic structure model is shown in Fig. 2(*b*) and the differences in the *R* values of the samples are shown in Table 2. While *R*3*c* exhibits an $a^-a^-a^-$ tilt system, the *P*1*m*1 phase exhibits an $a^-b^+c^-$ tilt system. A comparison of the two structure models in Figs. 2(*a*) and 2(*b*) and **the inset of the $\frac{1}{2}310_C$ and $\frac{1}{2}311_C$ reflections [where is this?]** clearly show that only a combination of the two phases allows the correct modelling of the measured intensities. At low temperatures (5–150 K), however, the diffraction data were refined using a single-phase rhombohedral model with *R*3*c* space group only. Here a low-temperature structure of simple rhombohedral symmetry changes to a highly complex monoclinic structure at a higher temperature (Zhang *et al.*, 2009; Baker *et al.*, 2009*b*). This appears to be extremely unusual for most materials but it is the case with KNN ceramics, especially the Na-rich portion of the phase diagram.

In Glazer's (1972) notation, the *R*3*c* space group has $a^-a^-a^-$ anti-phase tilting of the oxygen octahedra. Megaw & Darlington (1975) reported that, for rhombohedral perovskites, **the hexagonal axes should be used for the refinement, which allows for several important structural parameters to be determined**. The fractional coordinates for the hexagonal setting are shown in Table 3.

The geometrical relationships shown for rhombohedral *R*3*c* perovskites are used to calculate the structural parameters from the refinement results. The results of the Rietveld refinement are shown in Table 4. For diffraction data acquired at 5 and 150 K, respectively, the trigonal crystal structure with space group *R*3*c* best describes the observed diffraction data. At 300 K, there is phase coexistence between the trigonal and the monoclinic structure with space group *P*1*m*1, while at

Table 3
Fractional coordinates for the hexagonal setting of rhombohedral perovskites with space group *R*3*c*.

Atom	*x*/*a*	*y*/*b*	*z*/*c*
Na/K	0	0	1/4 + *s*
Nb	0	0	*t*
O	1/6 − 2*e* − 2*d*	1/3 − 4*d*	1/12

526 K, only the monoclinic *P*1*m*1 best describes the observed pattern. The phase coexistence is an indication of a first-order phase transition with increasing temperature. From 776 to 976 K, the cubic structure with space group $Pm\bar{3}m$ best describes the diffraction pattern. The fraction of the phases at 300 K is 16.26% for the rhombohedral phase and 83.74% for the monoclinic phase. The density values for the sample decrease with increasing temperature, from 4.555 (5) g cm^{-3} at 5 K to 4.434 (1) g cm^{-3} at 976 K. The refinement parameters for the sample show a good agreement from very low temperatures up to high temperatures.

The lattice constants for the sample as a function of measurement temperature are shown in Fig. 3(*a*). It appears as

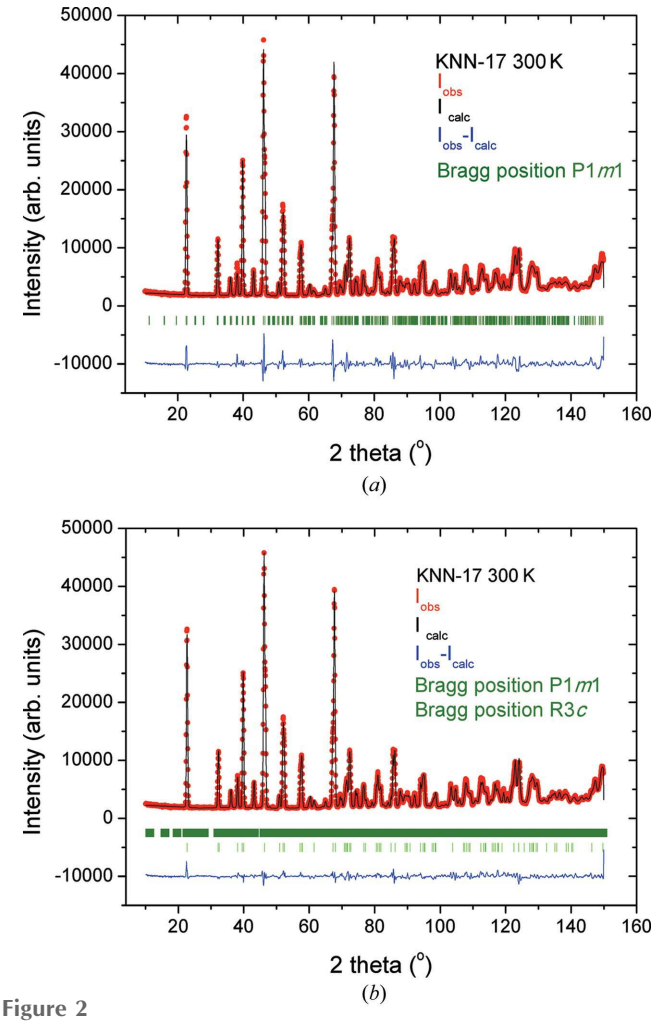

Figure 2
Measured and calculated neutron diffraction profiles and their difference curves for $(K_{0.17}Na_{0.83})NbO_3$ ceramics at 300 K

if the values of the lattice parameters change a lot with increasing temperature, but a look at the unit-cell volume of the different structures shows a uniform increase with temperature. The parameters that give more information about the rhombohedral perovskite are based on the reports in the literature by Megaw & Darlington (1975) and later by Zhang *et al.* (2009). *s* describes the fractional displacement of the *A* cation along the lattice parameter *c* of the hexagonal cell (c_H) from the ideal perovskite structure site. Since the Na and K positions are fixed, a single *s* parameter is obtained. As the temperature of measurement increases, the displacement of Na/K along c_H increases but in the negative direction.

t measures the shift of the *B* cation along the same direction from the centre of the octahedron, and as the temperature of data acquisition increases, the Nb shift from the centre of the octahedron decreases. The rhombohedral angle α_{pc} in the pseudo-cubic cell is calculated from the relation

$$\cos\alpha_{pc} = (c_H^2 - 6a_H^2)/(c_H^2 - 12a_H^2), \quad (1)$$

where a_H and c_H are the lattice parameters. A graph of the cation displacements *s* and *t* as a function of temperature is shown in Fig. 3(*b*). The displacements of both *A* and *B* cations are negative as the temperature increases from 5 to 300 K. For the *A* cation, the value decreases from −0.2307 to −0.234, while for the *B* cation, the value is from 0.2655 to 0.264. This implies that the cations are displaced from the cubic positions, indicating polarization of the unit cell and possibly ferroelectricity.

The lattice strain is the deviation of the rhombohedral angle from 90°. According to Thomas (1996), when the rhombohedral angle is less than 90°, **it [what is 'it' referring to here?]** conforms to the general behaviour of rhombohedral ferroelectric perovskites. The obtained rhombohedral angles are less than 90°, which implies that they exhibit ferroelectric behaviour. As the temperature increases, the values approach 90°, which means that the structure evolves towards cubic symmetry. *e* shows the rotation of the octahedron face about the triad axis, leading to the tilt angle ω according to the equation $\tan\omega = 4(3^{1/2})e$. A plot of the octahedral distortion *d* and the octahedral rotation *e* as a function of temperature is shown in Fig. 3(*c*). The trend for both distortions is negative with temperature. With increasing temperature, the value of *e* decreases from 0.0264 to 0.0256, which implies that the rotation of the octahedral face decreases slightly. The tilt angle also slightly decreases with temperature. *d* indicates the

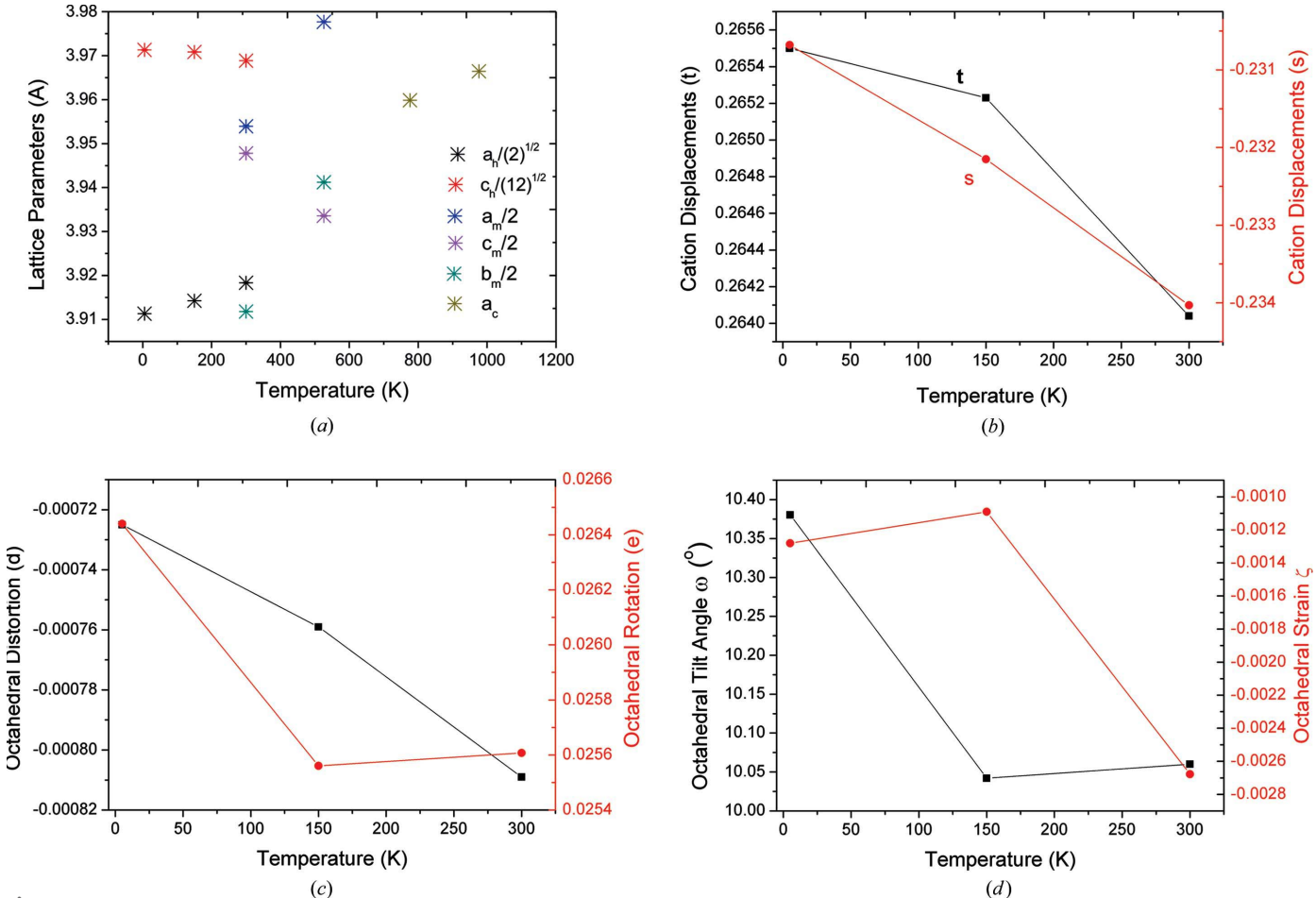

Figure 3
(*a*) Temperature dependence of the lattice parameters (Å) a_h, c_h for the rhombohedral phase, a_m, b_m, c_m for the monoclinic phase and a_c for the cubic phase for $(K_{0.17}Na_{0.83})NbO_3$ ceramics. (*b*) Cation displacements *s* and *t* as a function of temperature. (*c*) Octahedral distortion *d* and rotation *e* as a function of temperature. (*d*) Octahedral tilt angle ω and octahedral strain ζ as a function of temperature.

Table 4
Refinement results for $(K_{0.17}Na_{0.83})NbO_3$ ceramics from 5 to 976 K.

Temperature (K)	5	150	300		526	776	976
Crystal Structure	Trigonal	Trigonal	Trigonal	Monoclinic	Monoclinic	Cubic	Cubic
Space group	*R*3*c*	*R*3*c*	*R*3*c*	*P*1*m*1	*P*1*m*1	$Pm\bar{3}m$	$Pm\bar{3}m$
a (Å)	5.53143 (4)	5.53562 (4)	5.54137 (12)	7.9078 (3)	7.95538 (12)	3.95985 (3)	3.96645 (3)
b (Å)				7.82363 (12)	7.88237 (15)		
c (Å)	13.75702 (12)	13.75539 (12)	13.7485 (4)	7.89555 (20)	7.86712 (18)		
β (°)				90.3813 (11)	89.912 (2)		
Volume (Å^3)	364.527 (5)	365.037 (5)	365.613 (16)	488.47 (2)	493.325 (16)	62.0923 (7)	62.4029 (8)
Phase fraction (%)			16.26 (4)	83.74 (7)			
Density (g cm^{-3})	4.555 (5)	4.548 (5)	4.541 (2)	4.532 (2)	4.487 (2)	4.456 (1)	4.434 (1)
Z	6	6	6	8	8	1	1
Refinement							
R_p	7.78	8.36	9.39		11.7	16.2	15.3
R_{wp}	8.96	9.23	10.3		13.3	17.4	17.1
R_{exp}	2.57	2.7	2.99		2.83	2.91	2.72
χ^2	12.15	11.65	11.86		21.98	36.02	39.71
No. of data points	3060	3060	3060		3060	3060	3054
No. of parameters	28	28	46		38	19	19
t	0.2655	0.26523	0.26404				
s	−0.23068	−0.23215	−0.23403				
d	−0.000725	−0.000759	−0.000809				
e	0.02644	0.02556	0.025607				
α_{pc} (°)	89.4156	89.4207	89.5087				
w (°)	10.3804	10.0421	10.06				
ζ	−0.0012815	−0.001091	−0.0026775				
ω_a			4.301		1.613		
ω_b			7.466		6.047		
ω_c			3.038		0.965		

octahedral distortion where the triad axis symmetry is in place but the upper and lower faces are different. The values of *d* are negative, and this means that the upper face of the octahedron is larger than the lower face. The cation displacements are all positive, implying that Nb atoms move towards the upper large face. The octahedral strain (ζ) describes the elongation or compression of the octahedron along the triad axis and is given by the expression

$$1 + \xi = \cos w \left[\frac{c_H}{a_H (6)^{1/2}}\right]. \quad (2)$$

A graph of the octahedral tilt angle ω and the octahedral strain ζ as a function of temperature is shown in Fig. 3(*d*).

The values of ζ are negative, which shows that the octahedra are compressed while the tilt angle decreases with increasing temperature.

After the refinements, the **values [which values?]** of some of the oxygen atoms and the lattice parameters were used to calculate the tilt angles (ω_a, ω_b and ω_c) in the monoclinic *P*1*m*1 phase. The tilt angles are actually proportional to the intensity of the superlattice reflections. As the temperature of the data acquisition increases, the tilt angles decrease (Table 4).

3.2. $(K_{0.35}Na_{0.65})NbO_3$ ceramics from 5 to 776 K

$(K_{0.35}Na_{0.65})NbO_3$ ceramics have a piezoelectric charge coefficient (d^*_{33}) value of 125 pm V^{-1}, a Curie temperature (T_c) of 685 K, a remanent polarization value of 24 µC cm^{-2}, and a coercive field E_C of approximately 6800 at 100 kHz and dielectric loss of 0.025 (Mgbemere *et al.*, 2009*b*).

The neutron powder diffraction patterns for $(K_{0.35}Na_{0.65})NbO_3$ ceramics from 5 to 776 K are shown in Fig. 4. Some superlattice reflections which lead to the tilting of the oxygen octahedra can be observed, especially for patterns at low temperatures. As the temperature of data acquisition increases, the diffraction patterns also gradually change, reflecting alterations in crystal structure from a mixture of rhombohedral and monoclinic phases at 5 K to a mixture of tetragonal phases at 776 K. *R* values from the Rietveld refinement of the various models investigated in this work are shown in Table 5. The models with the lowest *R* values are chosen to represent the observations in the diffraction patterns for the sample

The diffraction patterns and hence the refinement for $(K_{0.35}Na_{0.65})NbO_3$ ceramics are more complicated than for the $(K_{0.17}Na_{0.83})NbO_3$ composition, possibly because of the difference in stoichiometry between the actual and the expected amount of sodium in the sample. The details of the refinement results are shown in Table 6. It is common practice in the synthesis of KNN ceramics to add an excess of about 2–3 mol% of the alkali elements to compensate for volatiliza-

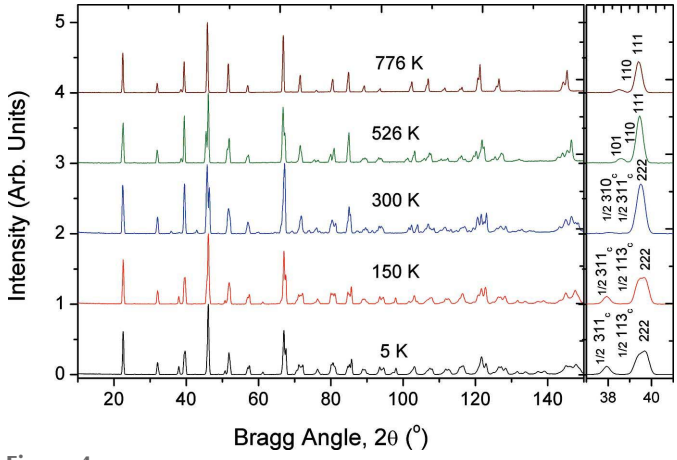

Figure 4
Neutron powder diffraction (λ = 1.5484 Å) patterns of $(K_{0.35}Na_{0.65})NbO_3$ at 5, 150, 300, 526 and 776 K. The right-hand panel shows some of the tilt peaks in the patterns between 37 and 41°, from 5 K to temperatures up to 300 K. The subscript 'c' refers to the pseudocubic indexing of the unit cell.

Table 5
Table showing the refinement details for all possible models investigated for $(K_{0.35}Na_{0.65})NbO_3$ ceramics from 5 to 776 K.

The models that were actually selected are shown in bold.

Temperature (K)	Space group	R_p	R_{wp}	χ^2	R_{Bragg}
5	*P*1*m*1	20.20	23.7	115	7.02
5	***P*1*m*1**	**6.93**	**7.23**	**9.82**	**3.46**
	R*3*c				**3.4**
5	*R*3*c*	36	36.9	245	22.3
150	*P*1*m*1	23.7	26.9	133	8.61
150	***P*1*m*1**	**12.1**	**12.9**	**27.9**	**5.8**
	R*3*c				**5.54**
150	*R*3*c*	36.4	38.2	241	22.5
300	***P*1*m*1**	**16.4**	**17.2**	**42.4**	**8.16**
526	***P*4*mm***	**10.6**	**12**	**11.7**	**5.98**
	P*4*mm				**5.51**
526	*P*4*mm*	18.1	18.2	26.8	6.26
776	*P*4*mm*	Negative Lorentzian: no convergence is achieved			
	*Pm*3*m*				
776	***P*4*mm***	**15.5**	**15.6**	**21.61**	**5.81**

tions during sintering. In the case of this sample, the chemical analysis showed that, while the amount of potassium was as expected, that of sodium was higher.

Phase coexistences can be observed in a broad range of temperatures from 5 to 776 K. At 5 K, the structure model was refined using a combination of monoclinic *P*1*m*1 and rhombohedral *R*3*c* space groups. The fractions of the phases are 48.79 and 51.21%, respectively. The monoclinic–rhombohedral phase coexistence was also observed at 150 K, the fractions of the phases being 44.35 and 55.65% **(Fig. 5)**. A single-phase monoclinic *P*1*m*1 model was used to refine the structure at 300 K. In order to verify the transition to a single monoclinic phase, a combined refinement with neutron and high-resolution X-ray diffraction data (PETRA III at DESY in Hamburg) was performed. The measured and calculated synchrotron diffraction profiles and their difference curves are shown in Fig. 6. A monoclinic *P*1*m*1 model is adequate to describe the observed patterns for both synchrotron and neutron data and gave good refinement fits. At 526 K, two tetragonal *P*4*mm* phases with slightly different lattice parameters gave a better refinement fit than only one tetragonal phase. A very small amount of the second tetragonal phase (3.35%) is necessary to achieve a good fit. It has been reported in the literature that changes in stoichiometry can cause a core–shell structure in KNN ceramics (Zhen & Li, 2007; Wang *et al.*, 2007). The core and the shell have different concentrations of the elements and thus slightly different structures, which might be a possible explanation of our observation. As the temperature increases to 776 K, the sample can still be refined using a tetragonal phase model. Considering the two phases at low temperatures, the density of the sample can be said to increase with increasing temperature.

The tolerance factor values for the $(K_{0.17}Na_{0.83})NbO_3$ and $(K_{0.48}Na_{0.48}Li_{0.04})(Nb_{0.86}Ta_{0.1}Sb_{0.04})O_3$ samples are 0.982 and 1.016, respectively. An investigation into the tolerance factor values for the proposed and actual composition of the $(K_{0.35}Na_{0.65})NbO_3$ sample can give an insight into the materials properties. The proposed composition has a tolerance factor of 0.997, while the actual composition has a tolerance factor of 1.03. According to Acker *et al.* (2010), non-stoichiometry in KNN-based ceramics plays a significant role in the structure of the sample. The coexistence of phases observed in this sample is possibly caused by the distortion of the crystal structure which is induced by the difference in tolerance factor.

At 5 K a density of 4.362 (5) g cm^{-3} and at 150 K a density of 4.371 (7) g cm^{-3} was obtained for the sample. The density values are 4.649 (2), 4.545 (2) and 4.469 (1) g cm^{-3} at 300, 526 and 776 K, respectively.

The temperature dependence of the lattice parameters for $(K_{0.35}Na_{0.65})NbO_3$ ceramics is shown in Fig. 7(*a*). In order to compare the lattice parameter values in one graph, the values of the monoclinic phase were divided by 2, while the ***a* and *c* values** of the rhombohedral phase were divided by the square roots of 2 and 12, respectively, to match the pseudocubic values.

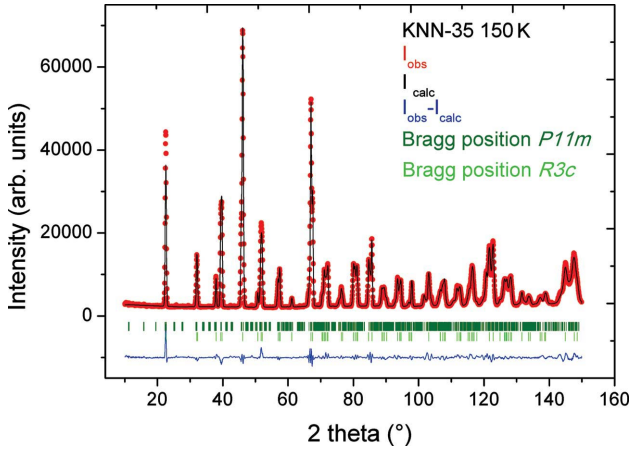

Figure 5
Measured and calculated neutron diffraction profiles and their difference curves for $(K_{0.35}Na_{0.65})NbO_3$ ceramics at 150 K

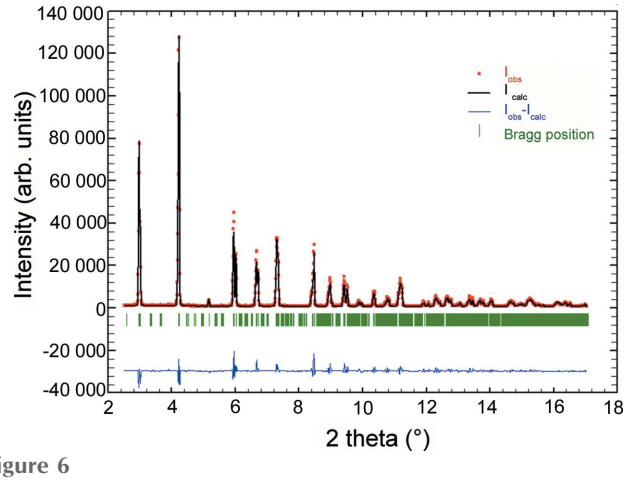

Figure 6
Measured and calculated diffraction profiles for a combination of neutron and synchrotron data and their difference curves for $(K_{0.35}Na_{0.65})NbO_3$ ceramics at 300 K.

A graph of the cation displacements s and t as a function of the temperature is shown in Fig. 7(b).

The displacement of the A-site cations along c_H shows that they are displaced in the negative direction, while there is a positive shift of the B-site cation along the same direction from the centre of the octahedron. The rhombohedral angles are less than 90°, which indicates the possible presence of ferroelectricity in the samples. A plot of the octahedral distortion d and the octahedral rotation e as a function of temperature is shown in Fig. 7(c). The positive value of ζ for the sample shows that the octahedra are elongated along the triad axis.

A graph of the octahedral tilt angle ω and the octahedral strain ζ as a function of the temperature is shown in Fig. 7(d).

When the tilt angles are **all negative or all positive**, its significance is relatively reduced, but tilt angles with different signs might show some trend. For the $(K_{0.35}Na_{0.65})NbO_3$ ceramics, the tilt angles do not show a clear trend. This might be due to the divergence from the stoichiometric composition (Mgbemere *et al.*, 2009*a*) which led to the coexistence of phases at most temperatures of data acquisition.

3.3. $(K_{0.48}Na_{0.48}Li_{0.04})(Nb_{0.86}Ta_{0.1}Sb_{0.04})O_3$ ceramics from 5 to 300 K

The properties of KNN ceramics modified with Li, Ta and Sb have been reported by a lot of researchers (Fu *et al.*, 2008; Akdoğan *et al.*, 2008; Hagh *et al.*, 2008; Saito *et al.*, 2004; Mgbemere, Fernandes *et al.*, 2011). These properties vary with both the composition and the processing conditions. The measured d_{33} values range from 220 to 345 pC N^{-1}, while the T_c values range from 513 K to approximately 573 K. The dielectric constant values are as high as 1570 at room temperature with low dielectric loss. The dielectric constant values at room temperature have been calculated to be approximately 670 with a dielectric loss value of 0.029.

The neutron powder diffraction patterns for $(K_{0.48}Na_{0.48}Li_{0.04})(Nb_{0.86}Ta_{0.1}Sb_{0.04})O_3$ ceramics from 5 to 300 K are shown in Fig. 8. The right-hand panel is an enlargement of the patterns from 110 to 125° to highlight their differences with increasing temperature. No superlattice reflections are observed in the sample, which could possibly be a result of the doping with Li, Ta and Sb and the high amount of potassium in the sample. According to Baker *et al.* (2009*a*), when the

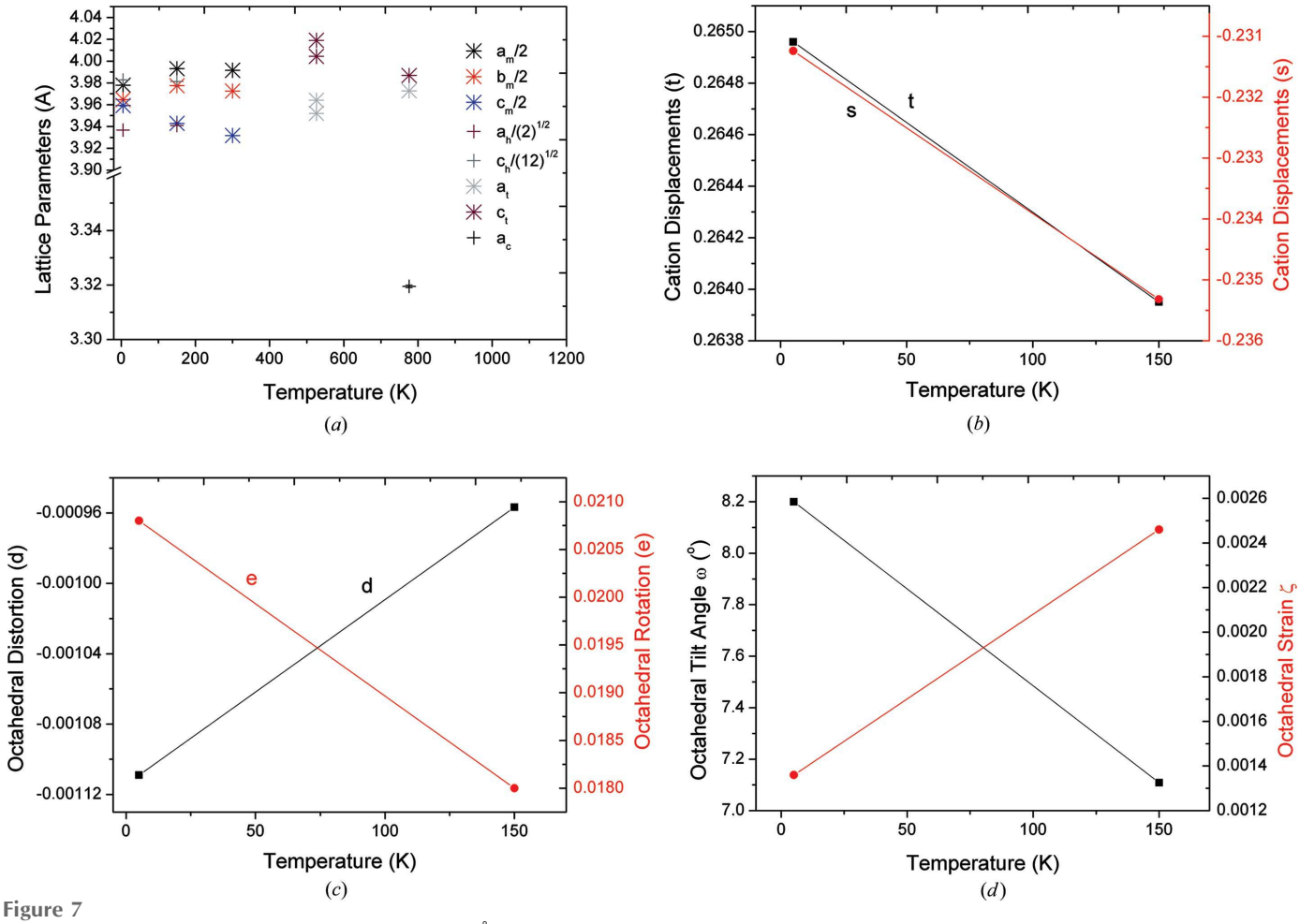

Figure 7
(*a*) Temperature dependence of the lattice parameters (Å) a_h, c_h for the rhombohedral phase, a_m, b_m, c_m for the monoclinic phase, a_t, c_t for the tetragonal phase and a_c for the cubic phase for $(K_{0.35}Na_{0.65})NbO_3$ ceramics. (*b*) Cation displacements s and t as a function of temperature. (*c*) Octahedral distortion d and rotation e as a function of temperature. (*d*) Octahedral tilt angle ω and octahedral strain ζ as a function of temperature.

Table 6
Refinement results for $(K_{0.35}Na_{0.65})NbO_3$ ceramics from 5 to 776 K **[should the cubic space group be $Pm\bar{3}m$?]**.

Temperature (K)	5		150		300	526		776	
Crystal system	Monoclinic	Rhombohedral	Monoclinic	Rhombohedral	Monoclinic	Tetragonal	Tetragonal	Tetragonal	Cubic
Space group	*P*1*m*1	*R*3*c*	P1*m*1	*R*3*c*	*P*1*m*1	*P*4*mm*	*P*4*mm*	*P*4*mm*	*Im*$\bar{3}$*m*
a (Å)	7.9559 (3)	5.56744 (4)	7.9862 (4)	5.57336 (6)	7.9832 (2)	3.96419 (5)	3.95204 (3)	3.97271 (3)	3.3195 (5)
b (Å)	7.9294 (3)		7.9549 (4)		7.94505 (16)	3.96419 (5)			
c (Å)	7.9184 (5)	13.79696 (20)	7.8857 (5)	13.7915 (3)	7.86360 (14)	4.01901 (7)	4.00434 (4)	3.98682 (7)	36.578 (10)
β (°)	90.421 (3)		90.086 (13)		90.2383 (20)				
Volume (Å^3)	499.52 (4)	370.361 (6)	500.98 (5)	371.002 (9)	498.76 (2)	63.1578 (15)	62.5424 (9)	62.9219 (14)	
Phase fraction (%)	48.79 (6)	51.21 (6)	44.35 (8)	55.65 (9)	100	3.35 (4)	96.65 (9)	100	0
Density (g cm^{-3})	4.143 (4)	4.57 (6)	4.131 (5)	4.562 (9)	4.649 (2)	4.502 (2)	4.547 (1)	4.469 (1)	
Z	8	6	8	6	8	1	1	1	1
Refinement									
R_p	6.93		12.1		16.4	10.7		15.5	
R_{wp}	7.25		12.9		17.2	12		15.6	
R_{exp}	2.31		2.44		2.64	3.52		3.36	
χ^2	9.82		27.9		42.39	11.52		21.61	
No. of data points	3020		3020		3020	3099		3099	
No. of parameters	36		36		38	29		30	
t	0.26496		0.26395						
s	−0.23124		−0.23532						
d	−0.001109		−0.0009567						
e	0.0208		0.018						
α_{pc}	89.5539		89.61						
w (°)	8.2		7.1085						
ζ	0.00136		0.00246						
ω_a (°)	−3.589		−2.261		−0.714				
ω_b (°)	−0.037		−1.406		3.718				
ω_c (°)	−2.106		−0.557		−2.495				

amount of potassium in the unmodified KNN solid solution is up to 40 mol%, the tilts disappear.

The measured and calculated neutron diffraction profiles and their difference curves for $(K_{0.48}Na_{0.48}Li_{0.04})(Nb_{0.86}Ta_{0.1}Sb_{0.04})O_3$ ceramics at 300 K are shown in Fig. 9. From the diagram, it is clear that the monoclinic *P*11*m* model adequately describes the measured diffraction pattern. The differences in the *R* values of the samples are shown in Table 7.

The refinement results for $(K_{0.48}Na_{0.48}Li_{0.04})(Nb_{0.86}Ta_{0.1}Sb_{0.04})O_3$ ceramics from 5 to 300 K are shown in Table 8. At 5, 150 and 300 K, the monoclinic *P*11*m* space group model was

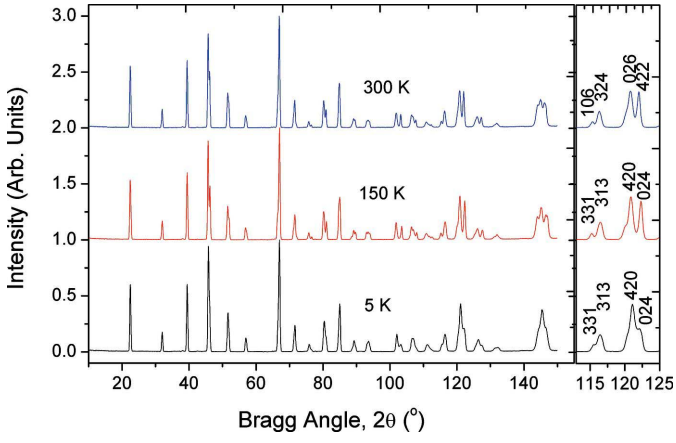

Figure 8
Neutron powder diffraction (λ = 1.5484 Å) patterns of $(K_{0.48}Na_{0.48}Li_{0.04})(Nb_{0.86}Ta_{0.1}Sb_{0.04})O_3$ at 5, 150 and 300 K. The right-hand panel shows some of the differences in the patterns between 110 and 125° with temperature.

Table 7
Table showing the refinement details for all the possible models investigated for $(K_{0.48}Na_{0.48}Li_{0.04})(Nb_{0.86}Ta_{0.1}Sb_{0.04})O_3$ ceramics from 5 to 776 K.

The models that were actually selected are shown in bold.

Temperature (K)	Space group	R_p	R_{wp}	χ^2	R_{Bragg}
5	***P*11*m***	**7.75**	**7.95**	**14.6**	**2.79**
5	*Amm*2	9.8	10.4	24.6	3.89
150	***P*11*m***	**6.38**	**6.48**	**9.23**	**2.72**
150	*Amm*2	16.8	20.3	88.2	5.62
300	***P*11*m***	**5.94**	**5.68**	**6.52**	**2.46**
300	*Amm*2	6.49	6.37	8.16	3.17
300	*R*3*c*	4.96	5.67	7.21	0.121
	*Amm*2				0.036

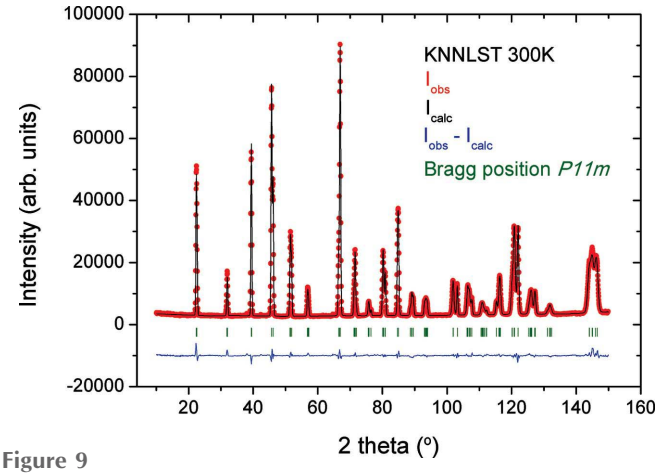

Figure 9
Measured and calculated neutron diffraction profiles and their difference curves for $(K_{0.48}Na_{0.48}Li_{0.04})(Nb_{0.86}Ta_{0.1}Sb_{0.04})O_3$ ceramics at 300 K.

Table 8
Refinement results for $(K_{0.48}Na_{0.48}Li_{0.04})(Nb_{0.86}Ta_{0.1}Sb_{0.04})O_3$ ceramics from 5 to 300 K.

Temperature (K)	5	150	300
Crystal Structure	Monoclinic	Monoclinic	Monoclinic
Space group	*P*11*m*	*P*11*m*	*P*11*m*
a (Å)	3.98263 (7)	3.98737 (7)	3.98728 (8)
b (Å)	3.98427 (10)	3.99029 (6)	3.98939 (7)
c (Å)	3.95270 (3)	3.944541 (16)	3.951368 (14)
γ (°)	89.7403 (8)	89.7148 (4)	89.7644 (4)
Volume (Å^3)	62.7204 (20)	62.7599 (15)	62.8532
Phase fraction (%)	100	100	100
Density (g cm^{-3})	4.7 (2)	4.697 (2)	4.812 (1)
Z	1	1	1
Refinement			
R_p	7.75	6.56	5.94
R_{wp}	7.95	6.5	5.68
R_{exp}	2.08	2.18	2.23
χ^2	14.57	8.862	6.52
No. of data points	3020	3020	3020
No. of parameters	37	37	37

used to refine the diffraction pattern. The orthorhombic *Amm*2 model also gave good refinement results at 300 K, but the *R* values are slightly lower. At 5 K, the density obtained is 4.70 (2) g cm^{-3}, and it gradually decreases to 4.697 (2) g cm^{-3} at 150 K and finally to 4.812 (1) g cm^{-3} at 300 K. Very reasonable refinement parameters are obtained for all the phases. The lattice parameter values for the sample as a function of temperature for the sample are shown in Fig. 10. The information obtained from this work will give more insight into the development and tailoring of existing and future lead-free piezoceramics and will help to improve their piezoelectric properties so that they can compete favourably with currently used lead-based piezoceramics.

4. Conclusion

The structure of $(K_xNa_{1-x})NbO_3$-based ceramics produced through the conventional ceramics processing method has been investigated using neutron powder diffraction. Chemical analysis shows that the expected and actual compositions of the samples are similar, except for the $(K_{0.35}Na_{0.65})NbO_3$ sample where the difference was large. The structure of $(K_{0.17}Na_{0.83})NbO_3$ composition is similar to what has been reported in the literature. Between 5 and 150 K, the structure is trigonal, and at 300 K, it has a two-phase coexistence between a monoclinic and a trigonal phase. At 526 K, it is monoclinic, and it changes to cubic from 776 K and above. The sample with composition $(K_{0.35}Na_{0.65})NbO_3$ has a two-phase monoclinic–rhombohedral coexistence at 5 and 150 K. At 300 K, it is monoclinic, and from 526 K, it is tetragonal. For the $(K_{0.48}Na_{0.48}Li_{0.04})(Nb_{0.86}Ta_{0.1}Sb_{0.04})O_3$ composition, the monoclinic *P*11*m* adequately describes the diffraction pattern at both 5 and 150 K. At 300 K, an orthorhombic phase adequately describes the pattern. This study has given more insight into the structure of some KNN-based ceramics, especially those modified with Li, Ta and Sb, where high piezoelectric properties have been reported. A better understanding of the structure at different temperatures will help researchers to engineer compositions that will possibly replace lead-based piezoelectric ceramics in the future.

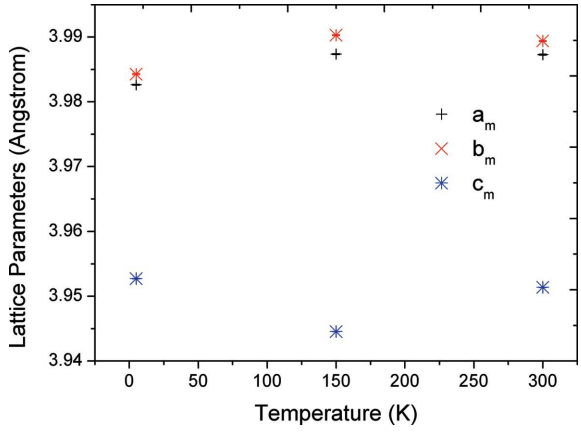

Figure 10
Temperature dependence of the lattice parameters (Å) a_m, b_m, c_m for the monoclinic phase in $(K_{0.48}Na_{0.48}Li_{0.04})(Nb_{0.86}Ta_{0.1}Sb_{0.04})O_3$ ceramics.

Acknowledgements

The research leading to these results has received financial support from the German Research Foundation (DFG) under grant No. SCHN 372/16:1-2.

References

Acker, J., Kungl, H. & Hoffmann, M. J. (2010). *J. Am. Ceram. Soc.* **93**, 1270–1281.
Ahtee, M. & Glazer, A. M. (1976). *Acta Cryst.* A**32**, 434–446.
Ahtee, M. & Hewat, A. W. (1975). *Acta Cryst.* A**31**, 846–850.
Ahtee, M. & Hewat, A. W. (1978). *Acta Cryst.* A**34**, 309–317.
Akdoğan, E. K., Kerman, K., Abazari, M. & Safari, A. (2008). *Appl. Phys. Lett.* **92**, 112908.
Baker, D. W., Thomas, P. A., Zhang, N. & Glazer, A. M. (2009*a*). *Acta Cryst.* B**65**, 22–28.
Baker, D. W., Thomas, P. A., Zhang, N. & Glazer, A. M. (2009*b*). *Appl. Phys. Lett.* **95**, 091903.
Egerton, L. & Dillon, D. M. (1959). *J. Am. Ceram. Soc.* **42**, 438–442.
Finger, L. W. (1998). *J. Appl. Cryst.* **31**, 111.
Finger, L. W., Cox, D. E. & Jephcoat, A. P. (1994). *J. Appl. Cryst.* **27**, 892–900.
Fu, J., Zuo, R., Wu, Y., Xu, Z. & Li, L. (2008). *J. Am. Ceram. Soc.* **91**, 3771–3773.
Glazer, A. M. (1972). *Acta Cryst.* B**28**, 3384–3392.
Haertling, G. H. (1967). *J. Am. Ceram. Soc.* **50**, 329–330.
Hagh, N. M., Jadidian, B., Ashbahian, E. & Safari, A. (2008). *IEEE-UFFC Trans.* **55**, 214–224.
Hoelzel, M., Senyshyn, A., Juenke, N., Boysen, H., Schmahl, W. & Fuess, H. (2012). *Nucl. Instrum. Methods Phys. Res. Sect. A*, **667**, 32–37.
Jaeger, R. E. & Egerton, L. (1962). *J. Am. Ceram. Soc.* **45**, 209–213.
Jenko, D., Bencan, A., Malic, B., Holc, J. & Kosec, M. (2005). *Microsc. Microanal.* **11**, 572–580.
Kodre, A., Tellier, J., Arčon, I., Malič, B. & Kosec, M. (2009). *J. Appl. Phys.* **105**, 113528.
Laar, B. van & Yelon, W. B. (1984). *J. Appl. Cryst.* **17**, 47–54.
Lallart, M. I. (2011). Editor. *Ferroelectrics – Material Aspects*. **Town of publication:** In Tech.
Lemeshko, M. P., Nazarenko, E. S., Gonchar, A. A., Reznichenko, L. A., Mathon, O., Joly, Y. & Vedrinskii, R. V. (2007). *Phys. Rev. B*, **76**, 134106.

Megaw, H. D. & Darlington, C. N. W. (1975). *Acta Cryst.* A**31**, 161–173.
Mgbemere, H. E., Fernandes, R. P., Hinterstein, M. & Schneider, G. A. (2011). *Z. Kristallogr.* **226**, 138–144.
Mgbemere, H. E., Herber, R.-P. & Schneider, G. A. (2009*a*). *J. Eur. Ceram. Soc.* **29**, 1729–1733.
Mgbemere, H. E., Herber, R.-P. & Schneider, G. A. (2009*b*). *J. Eur. Ceram. Soc.* **29**, 3273–3278.
Mgbemere, H. E., Hinterstein, M. & Schneider, G. A. (2011). *J. Appl. Cryst.* **44**, 1080–1089.
Mgbemere, H. E., Hinterstein, M. & Schneider, G. A. (2012). *J. Eur. Ceram. Soc.* **32**, 4341–4352.
Mgbemere, H. E., Hinterstein, M. & Schneider, G. A. (2013). *J. Am. Ceram. Soc.* **96**, 201–208.
Rodríguez-Carvajal, J. (2001). *IUCr Commission on Powder Diffraction Newsletter*, No. 26, pp. 12–19.
Rubio-Marcos, F., Bañares, M. A., Romero, J. J. & Fernandez, J. F. (2011). *J. Raman Spectrosc.* **42**, 639–643.
Saito, Y., Takao, H., Tani, T., Nonoyama, T., Takatori, K., Homma, T., Nagaya, T. & Nakamura, M. (2004). *Nature*, **432**, 84–87.
Shirane, G., Newnham, R. & Pepinsky, R. (1954). *Phys. Rev.* **96**, 581–588.
Shiratori, Y., Magrez, A. & Pithan, C. (2005). *J. Eur. Ceram. Soc.* **25**, 2075–2079.
Tennery, V. J. (1968). *J. Appl. Phys.* **39**, 4749.
Thomas, N. W. (1996). *Acta Cryst.* B**52**, 954–960.
Wang, Y., Damjanovic, D., Klein, N., Hollenstein, E. & Setter, N. (2007). *J. Am. Ceram. Soc.* **90**, 3485–3489.
Zhang, N., Glazer, A. M., Baker, D. & Thomas, P. A. (2009). *Acta Cryst.* B**65**, 291–299.
Zhen, Y. & Li, J.-F. (2007). *J. Am. Ceram. Soc.* **90**, 3496–3502.

JOURNAL OF APPLIED CRYSTALLOGRAPHY

ISSN: 1600-5767

ORDER FORM

YOU WILL AUTOMATICALLY BE SENT DETAILS OF HOW TO DOWNLOAD AN ELECTRONIC REPRINT OF YOUR PAPER, FREE OF CHARGE. PRINTED REPRINTS MAY BE PURCHASED USING THIS FORM.

Please scan your order and send to ls@iucr.org

INTERNATIONAL UNION OF CRYSTALLOGRAPHY
5 Abbey Square
Chester CH1 2HU, England.

VAT No. GB 161 9034 76

Article No.: J160519-KS5495

Title of article Neutron diffraction study of $(K_xNa_{1-x})NbO_3$-based ceramics from low to high temperatures

Name Henry Mgbemere

Address Institute of Advanced Ceramics, Hamburg University of Technology, Denickestrasse 15, Hamburg 21073, Germany

E-mail address (for electronic reprints) hmgbemere@unilag.edu.ng

OPEN ACCESS

IUCr journals offer authors the chance to make their articles open access on **Crystallography Journals Online**. For full details of our open-access policy, see http://journals.iucr.org/services/openaccess.html. For authors in European Union countries, VAT will be added to the open-access charge.

☐ I wish to make my article open access. The charge for making an article open access is **1000 United States dollars**.

DIGITAL PRINTED REPRINTS

I wish to order . . . . . paid reprints

These reprints will be sent to the address given above. If the above address or e-mail address is not correct, please indicate an alternative:

PAYMENT

Charge for open access **1000** USD Charge for reprints . . . . . USD Total charge . . . . . USD

☐ A cheque for . . . . . USD payable to **INTERNATIONAL UNION OF CRYSTALLOGRAPHY** is enclosed

☐ I have an open-access voucher to the value of . . . . . USD Voucher No.

☐ An official purchase order made out to **INTERNATIONAL UNION OF CRYSTALLOGRAPHY** ☐ is enclosed ☐ will follow

Purchase order No.

☐ Please invoice me

☐ I wish to pay by credit card

EU authors only: VAT No:

Date | Signature

OPEN ACCESS

The charge for making an article open access is **1000 United States dollars**. For authors in European Union countries, VAT will be added to the open-access charge.

A paper may be made open access at any time after the proof stage on receipt of the appropriate payment. This includes all back articles on **Crystallography Journals Online**. For further details, please contact support@iucr.org. Likewise, organizations wishing to sponsor open-access publication of a series of articles or complete journal issues should contact support@iucr.org.

DIGITAL PRINTED REPRINTS

An electronic reprint is supplied free of charge.

Printed reprints without limit of number may be purchased at the prices given in the table below. The requirements of all joint authors, if any, and of their laboratories should be included in a single order, specifically ordered on the form overleaf. All orders for reprints must be submitted promptly.

Prices for reprints are given below in **United States dollars** and include postage.

	Size of paper (in printed pages)				
Number of reprints required	1–2	3–4	5–8	9–16	Additional 8's
50	184	268	372	560	246
100	278	402	556	842	370
150	368	534	740	1122	490
200	456	664	920	1400	610
Additional 50's	86	128	178	276	116

PAYMENT AND ORDERING

Cheques should be in **United States dollars** payable to **INTERNATIONAL UNION OF CRYSTALLOGRAPHY**. Official purchase orders should be made out to **INTERNATIONAL UNION OF CRYSTALLOGRAPHY**.

Orders should be returned by email to ls@iucr.org

ENQUIRIES

Enquiries concerning reprints should be sent to support@iucr.org.